PAP-1040

Physical Hydraulic Modeling of Canal Breaches

By

Tony L. Wahl, Dale J. Lentz, Bruce D. Feinberg
U.S. Department of the Interior
Bureau of Reclamation
Technical Service Center
Hydraulic Investigations & Laboratory Services
Denver, CO

Dam Safety Conference 2011
Washington, D.C.
September 26-29, 2011

PHYSICAL HYDRAULIC MODELING OF CANAL BREACHES

Tony L. Wahl[1], Dale J. Lentz[2], Bruce D. Feinberg[3]

Abstract: Three physical hydraulic model tests were conducted to gain a better understanding of erosion and breach processes for canal embankments typical of irrigation canals constructed and operated by the Bureau of Reclamation. The testing investigated both piping and overtopping failure modes, the effects of a range of embankment erodibility characteristics, and unique aspects of the canal breaching situation that differ from the traditional breaching of embankment dams impounding large storage reservoirs. The testing provided data that confirms many similarities between the erosion processes that are important to canal breach and dam breach events. The tests also illustrated the importance of material erodibility parameters and breach development time to the estimation of peak breach outflows. Data obtained from these tests is supporting the development of tools for making appraisal-level predictions of canal breach outflow hydrographs.

Keywords: canal failure, embankments, canal breaches, outflow hydrographs, inundation levels, flooding, hydraulic modeling

Introduction

The Bureau of Reclamation (Reclamation) has constructed more than 8,000 miles of irrigation water delivery canals since 1902, and failures of canal embankments have occurred periodically throughout our history. Threats to these canals include animal burrows, tree roots, penetrations by turnout pipes and utilities, embankment and foundation issues, seismic events, internal erosion under static loading, hydrologic events, and operational incidents. Canal failures can have significant consequences, and the potential consequences increase over time as urban development surrounds formerly rural canals.

To evaluate the consequences of a canal breach, numerical modeling to estimate the breach outflow hydrograph and downstream flooding consequences is needed. Breaching of traditional embankment dams has been widely studied and tools for predicting dam breach outflow rates are reasonably well developed and continue to improve. However, breaching of canal embankments has not been studied extensively, and there are potentially significant differences between the canal situation and the embankment dam scenario. Most notably, the flow of water past the developing breach and limitations on the ability of the canal to convey water to the breach site may significantly affect erosion rates and the resulting breach outflow hydrograph.

To address questions about the differences between traditional dam breach and canal breach events, Reclamation is performing laboratory-scale physical model canal breach tests. The effects of varying material properties and different failure initiation mechanisms are being considered. Material erodibility is being quantified by in situ and laboratory submerged jet erosion testing. The long-term objectives are the development of both canal-specific breach

[1] Hydraulic Engineer, Bureau of Reclamation, Hydraulic Investigations and Laboratory Services Group, Denver, CO, twahl@usbr.gov.
[2] Hydraulic Engineer, Bureau of Reclamation, Hydraulic Investigations and Laboratory Services Group, Denver, CO.
[3] Hydraulic Engineer, Bureau of Reclamation, Flood Hydrology and Emergency Management Group, Denver, CO.

simulation models and simplified relationships for predicting canal breach outflow rates as a function of canal hydraulic properties, embankment geometry, and geotechnical/erodibility characteristics. Such tools will support both appraisal-level evaluation of large canal inventories and detailed analyses of specific cases.

Background

Although canal breaches have occurred throughout history, there have been remarkably few efforts to generalize experiences from these events. There is no guidance specific to canals for predicting breach parameters or breach outflow hydrographs, so the analyst at present is left with the option of applying equations developed for traditional embankment dams, or applying their own judgment in attempting to model a canal breach situation. Dun (2007) provided the most notable study of the hydraulics of a canal breach in a study of a navigation canal that failed in the United Kingdom in 2004. Dun proposed modeling the event with a combination of idealized hydraulic elements. Flow through the breach opening was modeled with a critical-flow section sized to match observed breach dimensions, and the breach flow was limited with two additional critical-flow sections located in the reaches of the canal upstream and downstream from the breach site. Breach initiation was modeled as an orifice-controlled outflow, since this particular breach was thought to have been initiated by piping through a badger den. Dun's calibrated model was able to reproduce the time series of observed water levels along the canal reaches, but Dun did not report the modeled outflow hydrograph from the breach, although the ability to predict breach outflow hydrographs for future failures was a stated motivation for the work. Dun concluded that the hydraulics of canal breaches were significantly different from breaches of traditional dams and storage reservoirs, with the discharge from dam breaches only limited by the breach geometry and reservoir storage, not by the upstream channel flow capacity.

Model Considerations

The previous work of Dun (2007) and consideration of the likely sequence of events and factors affecting the development of a canal breach led us to design a canal breach test facility that would simulate local canal and embankment geometry and hydraulic conditions for a breach located within an essentially infinite canal reach (no nearby check structures) and without the effects of any operational response by canal operators. The effects of an operational response and how it would interact with the hydrodynamics of the canal reach are difficult to include in a reasonably-sized physical model and are being addressed separately through numerical modeling. The physical model designed according to these principles could be considered to produce a worst-case scenario brought about by any of the following conditions or combinations of conditions:

- A long reach of canal between check structures with a large volume of water to be discharged through the breach before the canal can be shut down;
- A very rapid breach due to high erodibility rates for embankment materials;
- A slow operational response due to delayed detection of a failure in progress (e.g., a failure at night in a sparsely-populated area on a canal with little or no remote monitoring to indicate a failure in progress).

Figure 1 shows a plan view of the model test facility consisting of a 20-ft long erodible embankment test section connected to two nonerodible 25-ft long canal sections supplied with

water from individual head boxes in the laboratory. These canal sections represent the reaches that would be located upstream and downstream from a potential breach site. Since a canal breach can lead to reverse flow in the downstream section, each head box was supplied with enough water to meet the theoretical critical flow discharge that could occur toward the breach following an embankment failure. This critical discharge was determined for the specific energy present in the canal at its normal operating depth. At the start of a test, gates in each head box were set to waste most of this flow into bypass channels equipped with flow measurement weirs. The flow rates into the head boxes and into the waste channels were set so that the net flow past the erodible test section was equal to the Froude-scaled normal canal flow rate. As the breach developed during each test, the head box spill gates were then regulated to maintain a steady canal water level for as long as possible. This operational scheme maintained near-normal canal water depths in the model, thus simulating the slow draining of a large volume of water from an extended canal reach. The use of the gate-controlled waste channels relieved us from the need to vary the inflow to the model during a test. A photo of the test facility is shown in Figure 2.

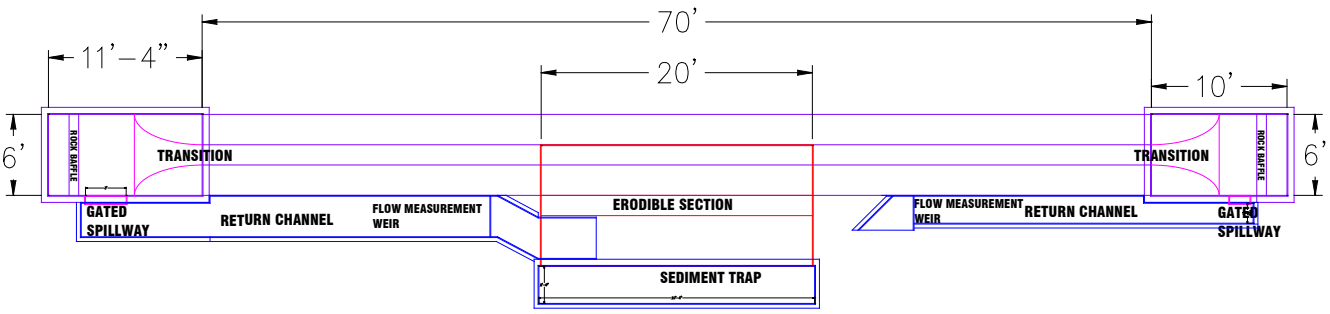

Figure 1. — Plan view of canal breach model test facility. Flow enters the canal via the head boxes at each end of the model. At the start of each test, the net flow in the canal is from right to left past the erodible embankment test section.

Figure 2. — Overview of canal breach model test facility, looking in the upstream direction.

The model canal and embankment cross-section is shown in Figure 3. It was designed as a 1:16 geometric scale model of an arbitrarily chosen 3,000 ft^3/s, concrete-lined, trapezoidal canal, although the model was constructed with homogeneous embankment sections with no concrete lining or any other simulated lining. The prototype canal cross section is a trapezoid with 24-ft base width, 1.5:1 (h:v) side slopes, a bed slope of 0.325 ft/mile (0.0000616 ft/ft) and a design Manning's *n* value of 0.014, yielding a normal flow depth of 16.4 ft. The model canal was constructed with no slope. Geometric scaling would have called for an elevation drop of 0.004 ft over the 70-ft length of the model, which was comparable to expected construction tolerances. The decision to not include a canal lining material was based on the fact that embankment breach typically takes place by headcutting, which progresses from the outboard side of the embankment toward the canal prism. Whether the driving force for erosion is an overtopping flow or piping flow through an existing flaw in the canal lining and embankment, failure takes place by erosion of embankment materials due to this flow. The lining simply collapses once the embankment has been eroded and all structural support for the lining is gone. The effect of the lining upon the critical erosion processes is minimal.

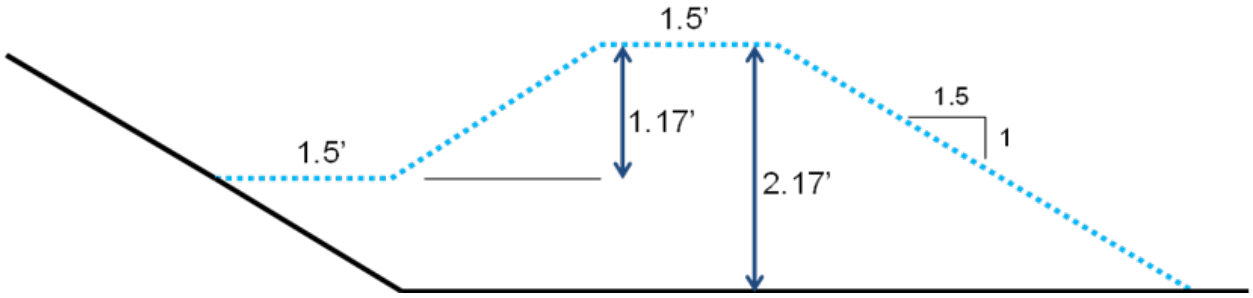

Figure 3. — Cross-section view of model canal and embankment test section.

The three tested embankments were constructed in the model as simulated fill sections in a canal reach that is elevated above the surrounding landscape. On the wetted side of the embankment, the embankment crests were 1.17 ft above the canal invert. On the land side of the embankment, the toe of the embankments was located 1.0 ft below the canal invert elevation. In this configuration, the breach is free to deepen below the canal invert, which will lead to the capturing of the full canal flow and the largest breach outflow.

Embankment Materials

All three test embankments were constructed from the same soil, a silty sand (SM) obtained from a local landscape materials supplier. To simulate the wide range of erodibility properties that we expect real canal embankments to exhibit, we varied both the water content at compaction and the level of compaction effort. The test soil contained enough clay fines that it exhibited some plasticity (PI=5) and its erodibility was sensitive to the placement conditions. To characterize the soil prior to placement, a standard Proctor compaction test was performed. Properties of the test soil are summarized in Table 1, the grain-size distribution curve is given in Figure 4.

Table 1. — Soil characterization.

Classification[a]	Grain size[b]			Plasticity Index, PI[c]	Standard Compaction[d]	
	% gravel	% sand	% fines		$\gamma_{d,max}$, lb/ft^3	w.c.$_{opt}$
SM – silty sand	6	69	25 (10% < 0.005 mm) (8% < 0.002 mm)	5	120.9	12%

Standards used to determine soil properties:
[a] ASTM D2487, USBR 5000
[b] ASTM D2487, USBR 5330
[c] ASTM D4318, USBR 5360
[d] ASTM D698A

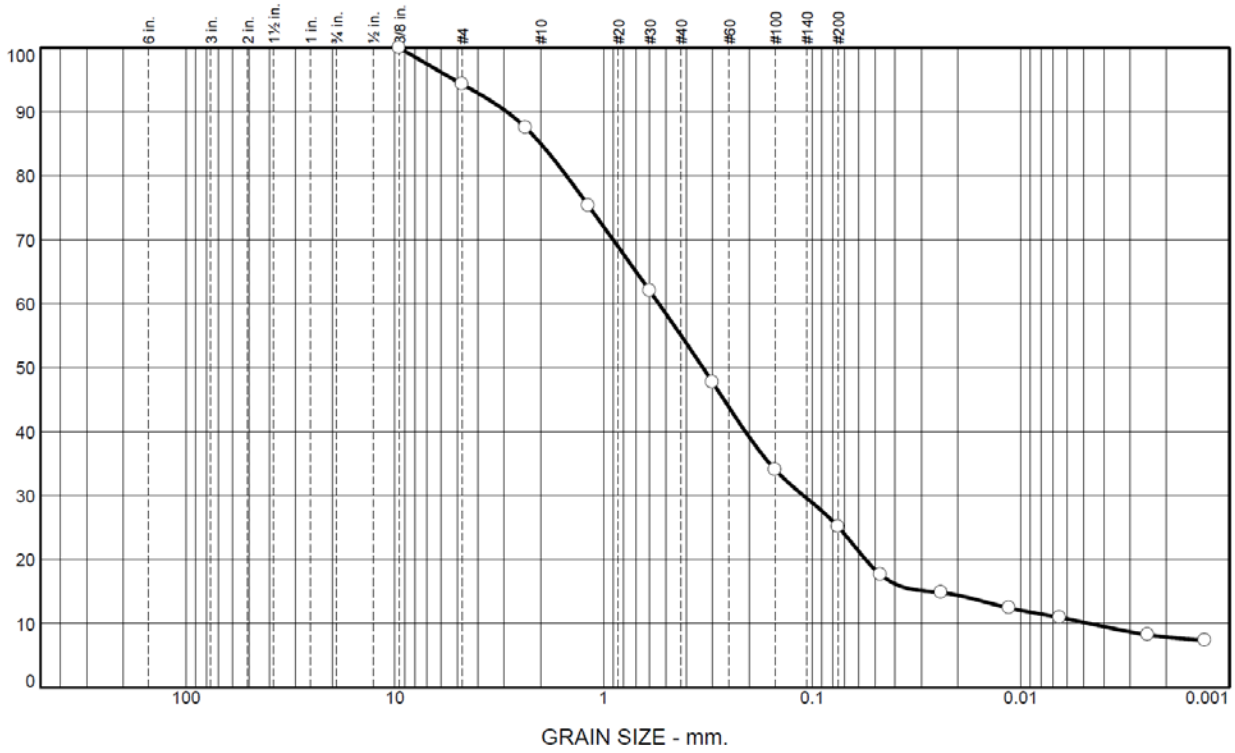

Figure 4. — Grain-size distribution curve for test soil.

Specimens prepared during the compaction test were evaluated for their erodibility using a submerged jet erosion test (Figure 5). This test measures the scour produced over time beneath a ¼-inch diameter submerged hydraulic jet impinging on the soil surface. Procedures for performing this test and analyzing the data to determine a jet index are described in ASTM Standard D5852 (2003). The current work used the ASTM test procedures, but the data were analyzed using the method of Hanson and Cook (2004), which produces values of the critical shear stress, τ_c, and the detachment rate coefficient, k_d, for a sediment detachment model expressed as

$$\dot{\varepsilon} = k_d\left(\tau - \tau_c\right) \tag{1}$$

In this equation, $\dot{\varepsilon}$ is the volume of material removed per unit surface area per unit time (units of velocity), τ is the applied shear stress, τ_c is the critical shear stress needed to initiate

sediment detachment, and k_d is the detachment rate coefficient (units of length per time per stress).

Figure 6 shows the results of the compaction and submerged jet tests, focusing on the detachment rate coefficient as the key parameter describing erodibility. For the Standard Proctor compaction effort, the optimum water content for compaction was about 12%, while the minimum erodibility was achieved at about 13% water content. On the wet side of optimum the erodibility increased about one half order of magnitude with a 5% increase in water content. On the dry side of optimum, erodibility increased more than 2 orders of magnitude with a water content reduction of about 6%. These results are consistent with similar testing by Hanson and Hunt (2007) on silty sand and lean clay soils. While the curves depict performance at standard compaction effort (12,375 ft-lb/ft^3), it should be noted that with lower compactive effort, the optimum water content for that level of compactive effort will typically increase. Figure 6 also shows the results of in situ sand cone density and submerged jet erosion tests carried out on the three tested embankments, which all received less than standard compaction effort and exhibited dry unit weights below the compaction curve. The erodibility of the test embankments is believed to be representative of the range of erodibilities possible in real canal embankments, such as those that are poorly compacted or constructed from inherently weaker materials such as non-plastic ML and SM soils. Hanson and Hunt (2007) showed that erodibility is strongly impacted by compaction effort, compaction moisture, and soil type, and very low and very high erodibility rates can result from many different combinations of those factors.

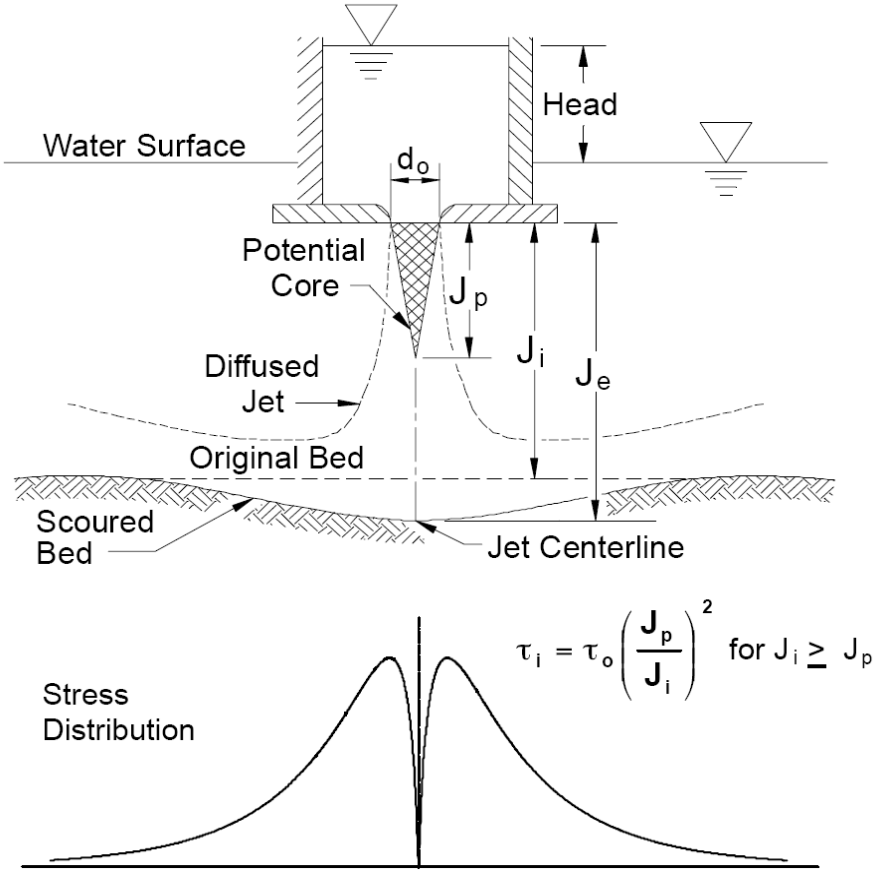

Figure 5. — Schematic of submerged jet test (from Hanson and Cook 2004).

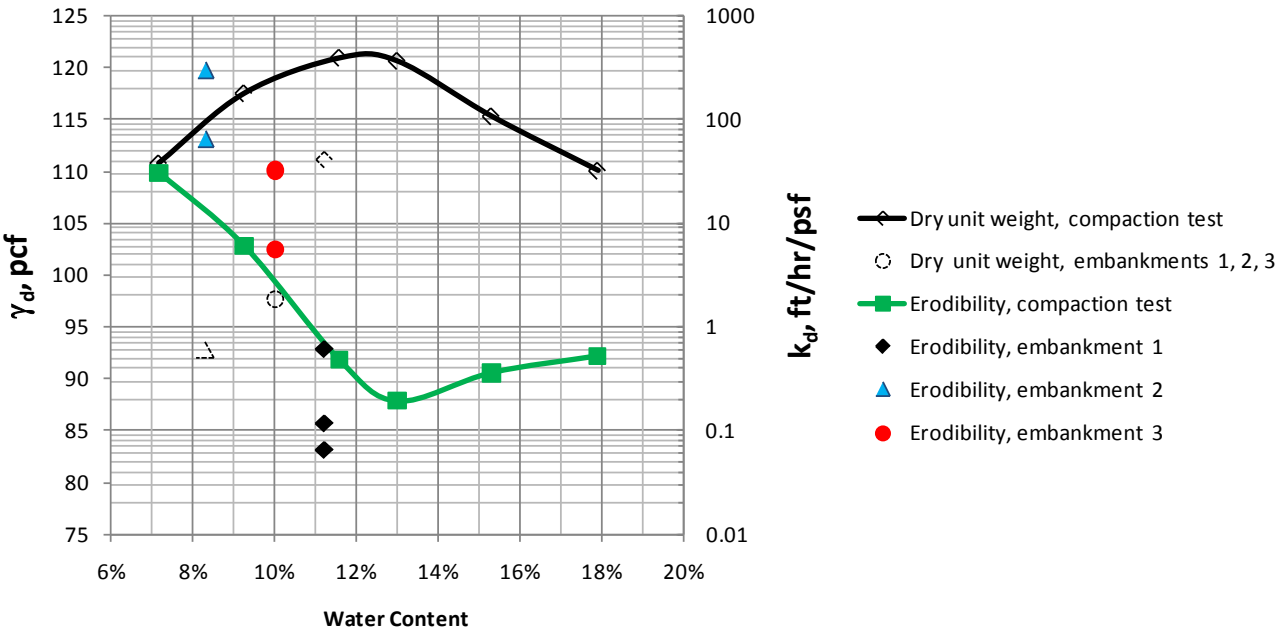

Figure 6. — Changes in dry unit weight, γ_d, and detachment rate coefficient, k_d, as a function of water content for Standard Proctor compaction test specimens and tested canal embankments.

Embankment Placement and Testing

Three embankments were constructed and tested during an 8-week period. The objectives were to test embankments that were relatively erosion resistant, moderately erodible and very erodible. The erosion resistant embankment was constructed and tested first, and the second embankment proved to be very erodible. The third embankment was intended to have erodibility midway between the first two embankments, but proved to be only marginally more erosion resistant than the second embankment.

Embankment construction began with soil being brought into the lab and stockpiled adjacent to the test facility where it was moistened and mixed using forklifts and front-end loaders. When the desired water content was reached, material was moved by conveyor into the test section and placed in 4- to 5-inch loose lifts, then compacted to about 3-inch lift thicknesses. Each lift of the first embankment was compacted with two passes of a vibratory plate compactor and one pass of a jackhammer with a shop-built, knobby compaction plate meant to produce kneading action similar to that of a sheepsfoot roller (Figure 7). The jackhammer device did the most to effectively compact the material. The second and third embankments received three and four passes of the vibratory plate compactor, respectively, and were not compacted with the jackhammer device. All of the embankments were constructed on top of a wood-framed support table which did not offer a firm base that would be typical of compaction over a solid ground surface. As a result, relatively low densities were achieved, especially for the second and third embankments.

As each embankment reached the canal invert elevation, placement was temporarily halted to allow a sand cone density test and in situ submerged jet test to be run (Figure 8).

Following the completion of these tests, the affected areas were re-filled and locally compacted, and the surface was scarified before continuing the placement operation. The planned failure mode for each embankment was piping, with the pipe initiated by embedding a #4 (½-inch diameter) rebar in the embankment at the desired elevation, passing completely through the embankment from the canal side to the land side. As the proper pipe elevation was reached, the rebar was placed and compacted into the embankment with subsequent lifts. This rebar was later pulled from the embankment to start the breaching process. When embankment material had been placed to the desired finished height, each embankment and associated canal section was trimmed and finished to match a template, and grid markings were then painted on the downstream face. Grid markings were painted on at 1 ft intervals horizontally, and at 0.5 ft intervals of elevation.

Figure 7. — Equipment used to compact test embankments.

Figure 8. — Performing *in situ* submerged jet erosion test.

Test Procedures

Tests were conducted by initiating flow into both head boxes at a predetermined flow rate of 8.5 ft^3/s, which was the model-scale critical flow discharge corresponding to the specific energy available in the canal at normal-depth flow conditions. The spill gates in each head box were initially set full open, and were then gradually throttled to bring the canal water surface up to normal depth and establish the normal flow rate (2.9 ft^3/s) past the embankment test section. Because of the possibility for seepage along the contacts of the embankment and the boundaries of the test section that might cause a premature breach, no attempt was made to hold these flow conditions long enough to establish a phreatic surface in the embankment. For most tests, only a few minutes was needed to establish the starting flow condition and get it stabilized. Once the flow was stable, the rebar was loosened and pulled out of the embankment to start the test.

Still photographs were taken before, during and after each test, and a continuous HD-quality video recording was made of each test from start to finish. Before and after each test, high-resolution photographs were taken for potential post-test analysis using photogrammetry software. In situ submerged jet tests were conducted following each test at suitable locations on the remnant embankment sections. For embankments 1 and 3, the post-breach erosion tests indicated somewhat more erosion resistance than the tests performed during embankment construction. For embankment 2 the post-breach test indicated greater erodibility, but this may have been due to the fact that the only available location to perform a test was on small remnant of the embankment's downstream slope, which may have been less effectively compacted.

Flow rates into the head boxes were held steady throughout each test using the laboratory's automatic flow control system, which utilizes venturi flow meters and a valve downstream from each meter regulated by a closed-loop controller. The meters are calibrated periodically using a weighing tank and have an estimated flow measurement uncertainty of ±0.5%. The discharge through the spill gate of each head box was measured using custom-built ramp flumes located in the channels that returned the waste flows back to the laboratory sump. Each ramp flume was equipped with an ultrasonic level sensor whose output was sampled and recorded on a 5-second interval with a PC-based data acquisition system. Knowing the constant inflow to each end of the model, the measurement of the wasted flows allowed the calculation of the net flow past the breach site, and the difference between the sum of the inflows and the sum of the wasted flows was the total breach outflow.

Water levels in the upstream and downstream canal reaches at the two ends of the 20-ft embankment test section were measured and recorded by the data acquisition computer. At the upstream ends of each canal reach (just downstream from the transitions from the head boxes into the canals), point gages were deployed to assist in maintaining steady water levels in the canals as the breach outflow increased. Gate adjustments in each test typically took place first at the downstream head box as the breach initiated, then in the upstream head box when canal levels could not be maintained by adjusting the downstream gate. This had the effect of not artificially increasing the upstream flow rate as the breach initially developed, but then allowed it to increase when there was significant canal drawdown at the breach site. No practical method of gate manipulations can exactly replicate the dynamics of a long canal reach, but this approach yielded canal flows that were representative of those that would occur in a prototype situation.

Embankment Test Summary

Three embankments were tested, with varying material erodibility parameters and different failure initiation details. Erosion rates were estimated from photo and video records and from physical measurements obtained during the tests. Table 2 gives a summary of the characteristics of the embankments and some observed erosion rates during periods of headcut advance into the embankments and breach widening. Complete details of the tests are given by Wahl et al. (2011).

Table 2. — Embankment characteristics and test observations.

Test	Compaction water content, %	γ_d, % of max	k_d, range of multiple tests, ft/hr/psf	Initial "pipe" elevation	Headcut advance rate, ft/min	Breach widening rate, ft/min
1	11.2	92	0.06 – 0.61	Canal invert	0.0006 – 0.006	0.0006 – 0.002
2	8.3	77	20 – 60	Canal invert	1.1	2.0
3	10.0	81	6 – 32	1.5 inches below canal water surface	0.02	0.64

Embankment 1 was very erosion resistant, compacted only about 1% dry of optimum and with the greatest compaction effort of all of the embankments. Failure of this embankment was initiated by removal of the rebar which had been embedded at the elevation of the canal invert. The hydraulic gradient on the piping hole was approximately 0.2 ft/ft. Development and advancement of a headcut through the embankment was very slow, prompting several interventions to attempt to accelerate the erosion process. The last intervention took place about 6 hours into the test, when an overtopping pilot channel was cut into the embankment. The test continued for another 15 hours after this, during which time the headcut advanced further into the canal and also widened, both at very slow and decreasing rates. This embankment never eroded rapidly enough to quickly release large volumes of water from storage in the canal, so a classical breach outflow "peak" never occurred. The breach outflow increased gradually in proportion to enlargement of the breach, and the maximum outflow from the breach was approximately 3.5 ft^3/s, about 120% of the normal canal flow rate. This maximum occurred only because we were providing greater than normal canal flow into the model and artificially working to maintain the normal canal water level. If this had been an actual canal failure, canal operators would have been able to shut down the canal as soon as breach outflow rates became noticeable, probably long before the breach outflow matched the normal canal flow rate.

Embankment 2 used the same failure mode as the initial testing of embankment 1, piping deep within the embankment at the canal invert elevation under a hydraulic gradient of about 0.2 ft/ft. This embankment was very erodible, as it was compacted about 3.5% dry of optimum and with the lowest compaction effort. The detachment rate coefficients for this embankment were about 3 orders of magnitude greater than for embankment 1. This embankment eroded very rapidly, with a headcut moving quickly into the embankment and the piping hole also seeming to enlarge rapidly at the same time during the first few minutes of the test. The embankment was fully breached within 8 minutes and the peak breach outflow reached 17 ft^3/s, the flow rate that was provided into the model. The equivalent peak breach outflow for the prototype would be 17,400 ft^3/s (1:16 scale), almost 6 times greater than the normal flow in the canal.

Embankment 3 was also relatively erodible, as it was compacted about 2% dry of optimum and with only slightly more compaction effort than embankment 2. The failure mode for this embankment was also piping, but the pipe was located high in the embankment, about 1.5 inches below the canal water surface (24 inches in a prototype 16 times larger than this model), with a hydraulic gradient of only 0.054 ft/ft. This is representative of an animal burrow or other defect that might occur at a higher elevation within the embankment. The low head on the pipe produced a very small flow that was able to cause headcutting into the embankment, but at a very slow rate (Figure 9). It took about 4.75 hours for this headcut to advance upstream to the embankment crest and breach into the canal prism. Although the flow rate out of the pipe was not directly measured, it did not appear to increase significantly during the time that headcut advancement was taking place, so we believe the hydraulic gradient and associated shear stress were too low in this test to cause enlargement of the hole. Once the headcut broke into the canal prism, breach development and widening (Figure 10) were very rapid and the breach reached the 17 ft^3/s peak outflow rate within about 4 minutes. This test illustrated the dramatic difference in erosion rates that can occur in the breach initiation phase and breach development phase as a result of the lower initial hydraulic gradient.

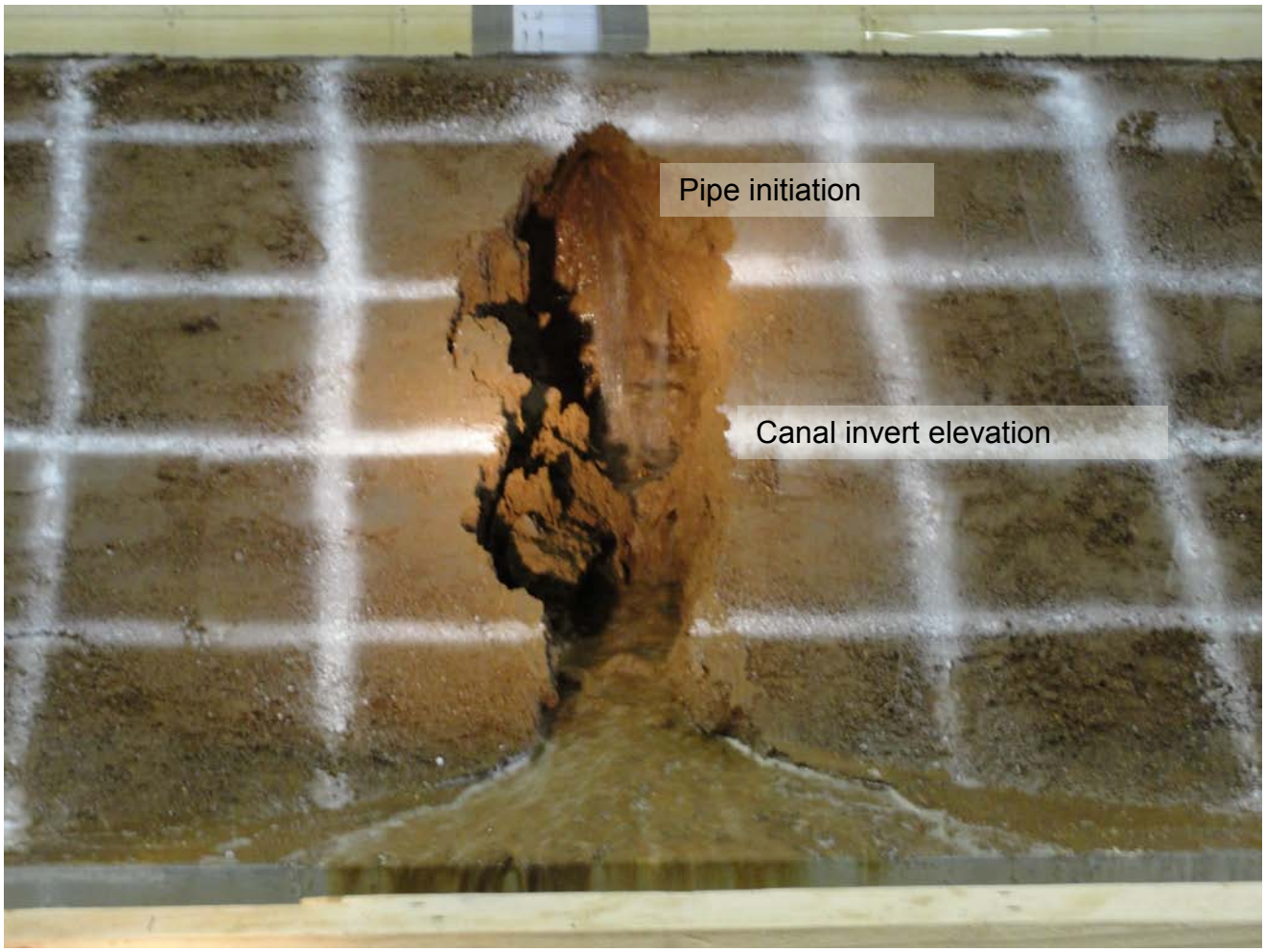

Figure 9. — Erosion of third embankment at t=3 hours. Note the flow through the pipe near the top of the headcut gully. At the middle of the photo, the second painted horizontal line from the bottom of the embankment is the canal invert elevation.

Figure 10. — Embankment number 3 eroding during breach development phase, following the collapse of the bridge over the initial piping hole. Original canal flow is right to left. The breach is progressing into the canal prism by continued headcutting through the upstream (canal-side) embankment slope, and widening due to a sequence of large mass-wasting events at the edges of the breach. One such mass failure is occurring at the upstream side of the breach (right side of photo).

Analysis

The fundamental erosion processes at work in these tests were pipe enlargement and headcutting into the embankment followed by breach widening. During the first phase of embankment failure (initiation), headcut advancement is the key process. During the second phase (breach development), widening is the key process, since widening of the breach directly increases the breach outflow until it becomes limited by the canal conveyance capacity. Some widening of the headcut does take place during the breach initiation phase, and some headcut advancement occurs at the beginning of the breach development phase, but in the simplest view the canal breach process can be subdivided into a just a two-step process of headcut advancement followed by breach widening. The SIMBA and WinDAM dam breach models (Temple et al. 2005, 2006) divide the breaching process further, recognizing a period of headcut advancement and breach enlargement into the reservoir between the breach initiation phase and the breach widening phase.

The three tests provided data that can be used to test existing relationships for modeling headcut advance and breach widening. A simple breach widening model proposed by Hunt et al. (2005) based on tests of embankment dam breaches undergoing pure breach widening is

$$\frac{dW}{dt} = 2k_d\left(\tau_{ew} - \tau_c\right) = 2k_d\left[0.7\gamma_w g\left(y_c^{1/3} n/1.49\right)^2 - \tau_c\right] \quad (2)$$

where *dW/dt* is the widening rate, τ_{ew} is the effective stress on the breach sidewalls, τ_c is the critical shear stress needed to initiate soil detachment, γ_w is the unit weight of water, y_c is the critical flow depth approximated as two thirds of the upstream flow depth, *n* is the Manning's *n* value within the breach opening, taken to be 0.020, *g* is the acceleration due to gravity, and 1.49 is a conversion factor needed to apply the equation in English units. This equation states that the erosion rate of each breach sidewall is proportional to k_d and the applied excess stress. Values of the critical shear stress, τ_c, are obtained from the submerged jet tests, although Hunt assumed τ_c=0 when developing the 0.7 factor that serves as a calibration factor and relates sidewall shear stress to bed shear stress. Applying this equation to periods of the three tests in which breach widening was occurring, the computed breach widening rates are shown in Table 3. The comparison between observed and predicted widening rates is good for the first test and fair for the second and third tests (within one order of magnitude), considering the variability of the materials (as exhibited by ranges of k_d values obtained from multiple jet tests) and other complicating factors. For the second and third tests, the predicted widening rates are somewhat lower than the observed rates.

Table 3. — Comparison of observed breach widening rates and those predicted using relation by Hunt et al. (2005).

Test	k_d (range) *ft/hr/psf*	τ_c *lb/ft²*	Computed breach widening rate (Hunt et al. 2005) *ft/min*	Observed widening rate during breach development *ft/min*
1	0.06 – 0.61	0.1	0.0002 – 0.002	0.0006 – 0.002
2	65 – 300	0.01	0.4 – 1.9	2.0
3	6 – 32	0.025	0.03 – 0.18	0.64

A simple headcut advance model that can be tested with the canal breach test data is the Temple/Hanson model (Temple et al. 2005), which relates the headcut advance rate to the rate of energy dissipation and material properties:

$$\frac{dX}{dt} = C\left(qH_h\right)^{1/3} \quad (3)$$

where *dX/dt* is the rate of headcut advance, *q* is the unit discharge in the headcut area, H_h is the vertical headcut height, and *C* is a material dependent advance rate coefficient. For each canal breach test, estimates were made of the unit discharge, headcut height, and advance rate, and the value of *C* for each test was then computed. Figure 11 shows these *C* values plotted against the associated ranges of k_d values measured from jet tests on each embankment, and compares the results to a relation proposed by Hanson et al. (2011) from flume headcut advance data originally reported in Hanson et al. (2001). The equation shown applies when k_d is specified in ft/hr/psf. (If k_d is given in customary metric units of $cm^3/(N\text{-}s)$, then the relation becomes $C=0.25k_d$ and the units of *C* are still $s^{1/3}/hr$.)

Agreement between the *C* vs. k_d values from the canal breach tests and the relation proposed by Hanson et al. (2011) is good, especially considering that these tests were affected by several complicating factors compared to the original flume headcut advance

experiments of Hanson et al. (2001). Embankment 2 exhibits the poorest fit to the relation and this may be due to the fact that headcut advance and piping hole enlargement seemed to take place simultaneously. This would tend to bias the headcut advance rate higher, which the figure shows. This is an encouraging result which suggests that the WinDAM model (Temple et al. 2006; Hanson et al. 2011) can be applied to the modeling of the erosion processes that occur during a canal embankment breach.

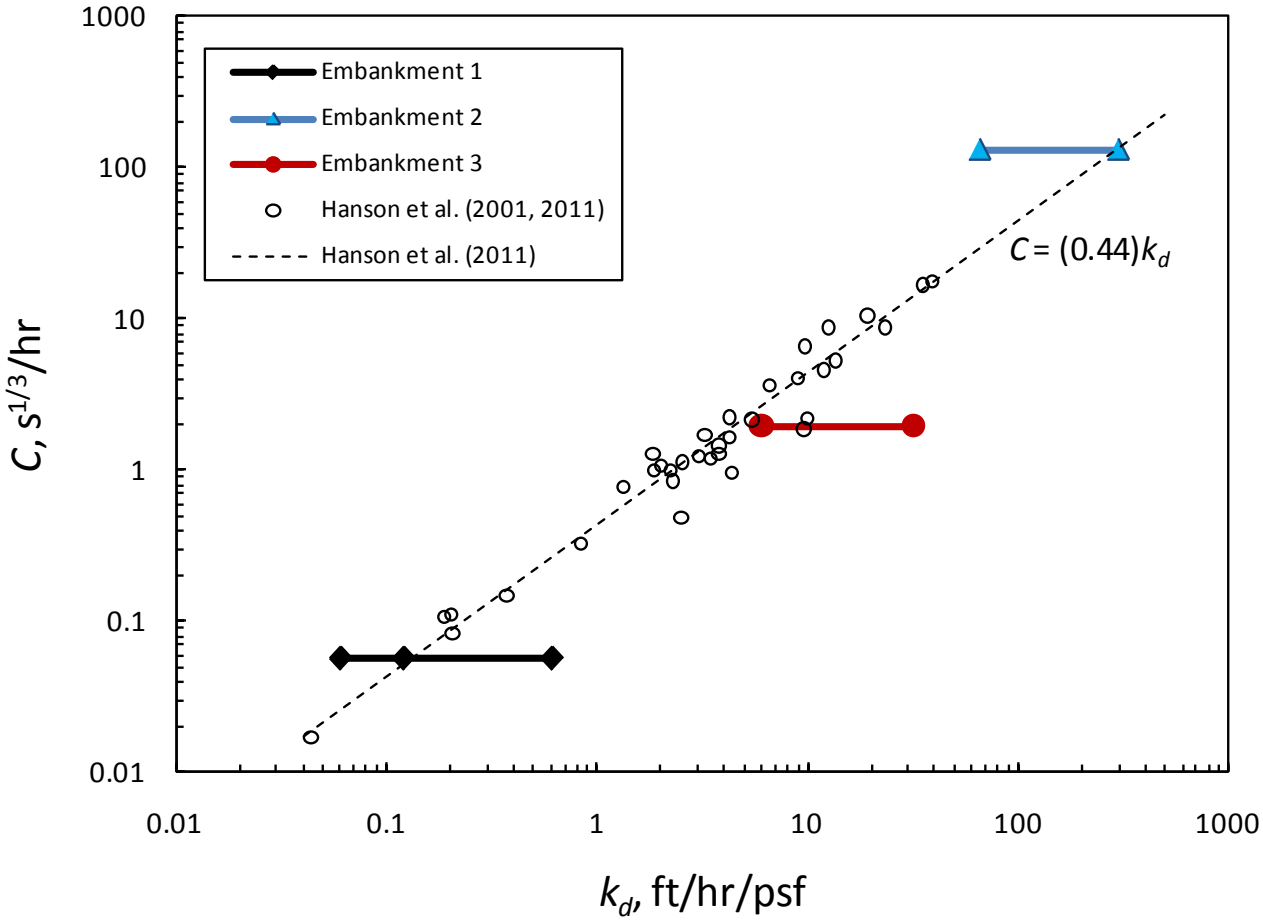

Figure 11. — Relation between headcut advance rate coefficients and soil detachment rate coefficients. Horizontal bars represent the range of pre-and post-test jet erosion test results for each embankment.

Conclusions

These canal embankment breach tests have demonstrated the variety of factors that can affect the development of a canal breach, including failure mode, material properties, and the different erosion mechanisms that are critical to each phase of the process. Erosion rate data from these tests compared well to existing relations for predicting headcut advance rate and breach widening rate as a function of measurable erodibility parameters. These results are useful for improving methods of estimating breach geometry and times for breach development.

Breach outflow rates from these tests are not directly applicable to prototype situations, since the boundary conditions of the physical model were configured to produce a worst-case scenario with respect to canal water levels and breach outflow rates. However, the tests did illustrate the important effect of the breach formation time on peak breach outflow. In the two tests with rapid breach development, peak outflows reached the maximum theoretical value that was forced upon the model, while in the one test with a slow breach development there was no significant peak in the outflow hydrograph. In a prototype case with such slow breach development there would have been ample opportunity to shut down the canal before a large breach outflow could occur. The key determinant of the breach development time is the erodibility of the embankment material, which is highly dependent on soil type, compaction effort, and water content at time of compaction. The key determinants of breach initiation time are the material erodibility and the hydraulic attack upon the embankment which can vary significantly as a function of the failure initiation mechanism and the associated flow rates. These tests provide data that could be used to propose a simple embankment erosion model to predict breach initiation time and breach development time. Such a model is now undergoing development and review.

Prediction of peak breach outflow rates requires modeling of both breach development processes and canal hydrodynamics. Changing breach development times will interact with the available canal storage, canal conveyance capacity and canal check structure boundary conditions to reduce the peak breach outflow from the maximum theoretical value. These issues are being explored in this research project through numerical modeling that is still underway.

The most rapid breach development and highest breach outflow rates will come from highly erodible embankments experiencing overtopping flow or piping under significant head. Erosion of these embankments will progress through the breach initiation phase relatively quickly and complete a rapid breach development before significant drawdown occurs in the canal. In this case, a reverse hydraulic gradient will be established in the downstream canal and flow will be supplied to the breach from both the upstream and downstream directions. The peak outflow in this case can approach two times the critical-flow capacity of the canal, which may be several times greater than the normal canal discharge. The short breach initiation time will limit opportunities for operational response, warning, or evacuation. Piping defects that are located higher in an embankment with lower seepage gradients may exhibit a longer breach initiation time. This can give more opportunity for detecting a breach in progress soon enough to take effective action to shut down the canal and reduce peak breach outflows.

Although soil erodibility rates spanned 3 orders of magnitude in these tests, cases of even higher and lower erodibility rates are possible due to variation of soil types and compaction conditions. In particular, many canals worldwide have been constructed from non-plastic silty sands. Future research should examine the breaching behavior of embankments constructed from such highly erodible materials.

References

1. ASTM, 2003. Annual Book of ASTM Standards, Section 4: Construction, Vol. 04.08. Philadelphia, Pa.: ASTM.
2. Dun, R.W.A., 2007. An improved understanding of canal hydraulics and flood risk from breach failures. *Water and Environment Journal.* 21(1): 9-18.
3. Hanson, G. J., K. M. Robinson, K. R. Cook. 2001. Prediction of headcut migration using a deterministic approach. *Transactions of the ASAE.* 44(3):525-531.
4. Hanson, G.J., and Cook, K.R., 2004. Apparatus, test procedures, and analytical methods to measure soil erodibility *in situ*. *Applied Engineering in Agriculture*, 20(4):455-462.
5. Hanson, G.J., and Hunt, S.L., 2007. Lessons learned using laboratory jet method to measure soil erodibility of compacted soils. *Applied Engineering in Agriculture*, 23(3):305-312.
6. Hanson, G.J., Temple, D.M., Hunt, S.L., and Tejral R.D., 2011. Development and characterization of soil material parameters for embankment breach. *Applied Engineering in Agriculture* (accepted for publication on March 22, 2011).
7. Hunt, S.L., Hanson, G.J., Cook, K.R., and Kadavy, K.C., 2005. Breach widening observations from earthen embankment tests. *Transactions of the ASAE*, 48(3):1115-1120.
8. Temple, D.M., Hanson, G.J., Nielsen, M.L., and Cook, K., 2005. Simplified breach analysis model for homogeneous embankments: Part 1, Background and model components. USSD Technologies to Enhance Dam Safety and the Environment, 25th Annual USSD Conference, Salt Lake City, Utah.
9. Temple, D.M., Hanson, G.J., and Nielsen, M.L., 2006. WINDAM – Analysis of overtopped earth embankment dams. ASABE Annual International Meeting, Portland, OR, 9 - 12 July 2006.
10. USBR, 1990. *Earth Manual, Part 2*, 3rd ed. U.S. Dept. of the Interior, Bureau of Reclamation, Materials Engineering Research Laboratory, Denver, CO.
11. Wahl, Tony L., Lentz, Dale J., and Feinberg, Bruce D., 2011. *Physical hydraulic modeling of canal breaches,* Hydraulic Laboratory Report *in press*, U.S. Dept. of the Interior, Bureau of Reclamation, Denver, CO.